Water and Environment Journal
Promoting Sustainable Solutions

CIWEM

Water and Environment Journal. Print ISSN 1747-6585

Preparation of layered double hydroxides using boron mud and red mud industrial wastes and adsorption mechanism to phosphate

Pan Hu[1], Yihe Zhang[1,2], Fengzhu Lv[1], Wangshu Tong[1], Hao Xin[1], Zilin Meng[1], Xinke Wang[1] & Paul K. Chu[2]

[1]Beijing Key Laboratory of Materials Utilization of Nonmetallic Minerals and Solid Wastes, National Laboratory of Mineral Materials, School of Materials Science and Technology, China University of Geosciences, Beijing 100083, China and [2]Department of Physics and Materials Science, City University of Hong Kong, Kowloon, Hong Kong, China

Keywords
adsorption; boron mud; LDH; phosphate; red mud.

Correspondence
Yihe Zhang, Beijing Key Laboratory of Materials Utilization of Nonmetallic Minerals and Solid Wastes, National Laboratory of Mineral Materials, School of Materials Science and Technology, China University of Geosciences, Beijing 100083, China.
Email: zyh@cugb.edu.cn
Fengzhu Lv, Beijing Key Laboratory of Materials Utilization of Nonmetallic Minerals and Solid Wastes, National Laboratory of Mineral Materials, School of Materials Science and Technology, China University of Geosciences, Beijing 100083, China.
Email: lfz619@cugb.edu.cn

doi:10.1111/wej.12212

Abstract

Phosphate removal was important for wastewater treatment, and adsorption was an efficient treatment process. In this study, the layered double hydroxide adsorbent (BR-LDH), which was prepared under alkali conditions using industrial residues boron mud and red mud, was used to adsorb the phosphate. The prepared BR-LDH was characterised by X-ray diffraction, Scanning electron microscopy, Energy-dispersive X-ray spectroscopy, and Thermo-gravimetric-differential thermal analysis. Adsorption experiments were carried out as a function of dosage, contact time, temperature and initial pH of phosphate solution. The removal ratio of phosphate onto OBR-LDH reached 93%. The adsorption data showed a good compliance with the pseudo-second-order kinetic model. In addition, the mineral composition, the functional groups, the valence of elements and zeta potentials of OBR-LDH before and after adsorption were used to analyse the adsorption mechanism. The result of real wastewater suggested that OBR-LDH was excellent adsorbent for phosphorus removal from actual wastewater.

Introduction

Phosphorus is widely used in agriculture and industry spurs the growth of photosynthetic algae and cyanobacteria (Delaney *et al*. 2011). Hence, excessive use of phosphorus poses many problems, notably eutrophication. When the concentration of phosphate in lakes or sea is over 0.03 mg/L, red tide occurs (Nijboer & Verdonschot 2004). Eutrophication leads to fish death and deterioration of habitats resulting in loss of plant and animal species (Håkanson *et al*. 2007). Therefore, wastewater must undergo treatment before discharging into the environment. Phosphates are mainly produced in household and industrial sewage because of the use of organic detergents. The typical municipal wastewater in the United States has a biochemical oxygen demand (BOD) for 5 days of 250 mg/L, chemical oxygen demand (COD) of 500 mg/L, and total phosphate of 12 mg/L. In Japan, the general wastewater standards for phosphate and nitrogen are 120 and 16 mg/L, respectively. In China, the urban sewage treatment standards for pollutant discharge secondary have a BOD for 5 days of 20 mg/L, COD of 60 mg/L, and total phosphate of 1.0 mg/L (Deng *et al*. 2014). In fact, the Chinese emissions standards for wastewater are stricter, especially for phosphates.

At present, physical, chemical and biological methods are used to remove phosphates (Ozacar 2003; Peleka & Deliyanni 2009). Chemical precipitation is the original and effective method for removing high concentration of phosphate, but suffers from variations in the effluent quality/quantity and sophisticated control systems are also required (Tillotson 2006). In comparison, biological removal methods are generally quite expensive and require complex aerobic effluent cycling for the complete treatment (Hesselmann

et al. 2000). In fact, adsorption is superior to the above techniques for removal of pollutants from aqueous solutions in terms of flexibility, design simplicity, operation flexibility and insensitivity to toxic pollutants while it also does not produce many harmful substances (Mustafa *et al*. 2006; Onyango *et al*. 2009; Roques *et al*. 1991).

Many kinds of adsorbents were investigated to remove phosphates, for instance, slag (Drizo *et al*. 2006), red mud (Huang *et al*. 2008), aluminum oxide, iron oxide (Zeng *et al*. 2004), calcite (Karageorgiou *et al*. 2007), dolomite (Roques *et al*. 1991), banana stems (Noeline *et al*. 2005), layered double hydroxides (LDHs) (Seida & Nakano 2002; Das *et al*. 2006; Yang *et al*. 2014). LDH, also known as hydrotalcite-like materials or anionic clays, had received much attention as an effective adsorbent. Its general formula is $[M^{II}_{1-x}\ M^{III}_{x}(OH)_2]^{x+}[A^{n-}_{x/n}\cdot mH_2O]^{x-}$, where M^{II} = Zn, Mg, Co, Ni, etc., M^{III} = Al, Fe, Cr, Ga, etc., $A^{n-} = CO_3^{2-}$, NO_3^-, Cl^-, SO_4^{2-}, etc. These are layered materials containing positively charged metal hydroxide sheets compensated by a large number of exchangeable charge-balancing anions and water molecules present in the interlayer space (Auerbach *et al*. 2004). Owing to the presence of large interlayer spaces and a huge number of exchangeable anions, LDH is very promising with respect to phosphorous uptake from wastewater.

Many literatures had reported that LDH could adsorb the heavy metals such as Pb, Cd, Cu and so on (Zhao *et al*. 2011; Rojas 2014; Huang *et al*. 2015). Meanwhile, there were also many literatures focusing on organics wastewater removal by LDH (Gök *et al*. 2014; Wang *et al*. 2015; Li *et al*. 2016; Zhang *et al*. 2016; Zhao *et al*. 2016). In addition, the few literatures which LDH treated the microorganisms in wastewater had been reported (Morris *et al*. 2008; Liu *et al*. 2013). However, the literatures focusing on real wastewater removal by LDH also had rarely been reported. Khitous *et al*. studied that removal of phosphate from industrial wastewater using uncalcined MgAl-NO_3 LDH and result showed the sorption capacity of 64.1002 mg/g (Khitous *et al*. 2015). In addition, phosphate ions were removed from aqueous solution using synthetic zeolite (Maurice et al. 2007).

In this study, we prepared RB-LDH by red mud and boron mud, which were industrial solid waste residue and cheaper than expensive chemical reagents. Red mud was a kind of solid waste residue with high pH (10–13) from the aluminum industry formed during bauxite. For every ton of alumina produced, approximately one to two tons (dry weight) of bauxite residues were generated. The corrosive nature of the red mud and its enormous quantities (90 million tons yearly worldwide) caused significant ecological problems and considerable negative environmental effects (Guo *et al*. 2014; Wang *et al*. 2014a,b). Boron mud was produced during the production of boric acid or borax. During the enrichment process of boron ores, a large quantity of boron mud was discharged and caused environmental contamination. Through calcining active red mud and boron mud, many minerals could be decomposed to active metal oxides. The active divalent and trivalent metal oxides could be used as the raw materials of RB-LDH. At present, the literatures about preparation of LDH using industrial solid wastes had seldom been reported. In the study, the prepared BR-LDH removed the phosphate from simulative wastewater and the removal ratio of phosphate could reached 93%.

Experimental details

Materials

The red mud was provided by Shandong Weiqiao Aluminum and Electricity Co., Ltd. (Shandong, China). Boron mud was supplied by Dandong Yilong Mining Co., Ltd. in Liaoning, China. The other reagents in this study were analytical grade.

Preparation of absorbent

A certain quantity of boron mud, red mud, and distilled water were added in a beaker and mixed thoroughly. The mixture was dried at 120°C and calcined at 600°C for 3 h. The sample was designated BR-600.

Sixty grams of BR-600 were added to a NaOH solution with a certain concentration to react at 30°C for 6 h. After aging for 24 h at room temperature, the sample was filtered and washed till the pH value of filtrate reached 7. Then, it was dried at 80°C and milled to form BR-LDH powders.

In order to determine the optimal preparation conditions for BR-LDH, the mass ratio of boron mud to red mud and the concentration of NaOH solution were studied in details.

Adsorption experiments

To assess phosphate adsorption, a stock solution was prepared with KH_2PO_4. The adsorption experiments were carried out in a 100 mL flask containing 50 mL of 100 mg/L KH_2PO_4 solution. The bottles were shaken in a digital water bath oscillator at 150 rpm. The influence of the contact time, temperature, and pH on adsorption were studied systematically. The initial pH value of the phosphate solution was adjusted by addition 0.1 mol/L of HNO_3 or 0.1 mol/L of NaOH. The concentration of phosphate was detected by the molybdate blue spectrophotometric method (Yan *et al*. 2010). The phosphate adsorption capacity q_e (mg/g) (1) and removal ratio R (%) (2) were derived from the following relationships:

$$q_e = \frac{(C_o - C_e)V}{m} \tag{1}$$

$$\mathrm{R} = \frac{C_o - C_e}{C_o} \times 100\% \tag{2}$$

where C_o and C_e are the initial and equilibrium concentration of phosphate in the solution (mg/L). q_e is the equilibrium

Table 1 The quality parameters of real wastewater from Qinghe sewage treatment plant in Beijing, China

Quality parameters	pH	Turbidity (NTU)	TSS (mg/L)	Soluble P (mg/L)	COD (mg/L)	Total N (mg/L)
Value	7.5	54	3	3.6	73	1.0

adsorption capacity (mg/g). *m* is the adsorbent dry weight (g) and *V* is the suspension volume (L).

In order to apply BR-LDH in the real wastewater, we collected real wastewater from Qinghe sewage treatment plant in Beijing, China. The quality parameters of the real wastewater were given in Table 1.

Characterisation

X-ray diffraction (XRD, Rigaku D/max-rA), Scanning electron microscopy (SEM, JSM-6301F), Thermo-gravimetric differential thermal analysis (TG, Netzsch TG-209C), Fourier transform infrared spectroscopy (FT-IR, PerkinElmer Spectrum 100) and Zetasizer analysis (Malvern Instruments Ltd., UK) were used to characterize the components, structure, morphology and charges of BR-LDH before and after adsorption.

Results and discussion

Analysis of raw materials

Boron mud and red mud

The mineral constituents and chemical composition of boron mud and red mud determined by XRD and XRF were shown in Table 2. The main constituents of boron mud were forsterite (Mg_2SiO_4), muscovite ($KAl_2(AlSi_3O_{10})(OH)_2$) and huntite ($Mg_{0.92}Ca_{0.08}CO_3{\cdot}3H_2O$). Red mud contained mainly gibbsite ($Al(OH)_3$), sodalite ($Na_4Al_3Si_3O_{12}Cl$), muscovite ($KAl_2(AlSi_3O_{10})(OH)_2$), hematite ($Fe_2O_3$) and goethite (α-FeOOH) (Atar *et al*. 2011; Yin *et al*. 2013). Through calcining active red mud and boron mud, many minerals could be decomposed to active metal oxides, such as MgO, Al_2O_3, Fe_2O_3, etc. for the preparation of LDH.

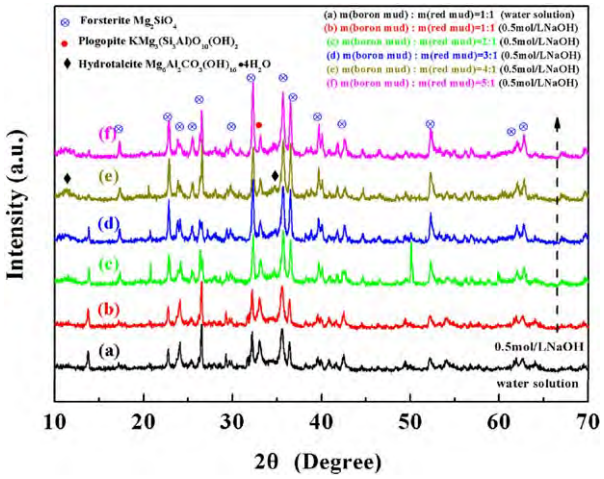

Fig. 1. XRD results of BR-LDH for different mass ratios of boron mud to red mud. [Colour figure can be viewed at wileyonlinelibrary.com]

Optimal preparation conditions for the BR-LDH

Effects of the mass ratio of boron mud to red mud

The proper ratio of divalent metal to trivalent metal was the key to forming the LDH crystalline structure. So the mass ratios of boron mud to red mud were investigated to the BR-LDH synthesis. Figure 1 showed the XRD results of BR-LDH with different mass ratios of boron mud to red mud (1 : 1, 2 : 1, 3 : 1, 4 : 1, 5 : 1). As shown in Fig. 1(a), BR-600 contained mainly forsterite and muscovite. Fig. 1(b)–(f) showed the XRD patterns for BR-600 with different mass ratios of boron mud to red mud with 0.5 mol/L NaOH. When the mass ratio reached 4 : 1, the peak at 11.46° corresponding to the (003) crystalline plate of LDH appeared gradually, but it was quite weak (Liao *et al*. 2012). This was due to the low concentration of NaOH. The following effects of NaOH concentration were studied.

Effects of NaOH concentration

Figure 2(a)–(g) showed the XRD patterns of BR-LDH for different concentrations of NaOH (0.5, 1, 2, 3, 4, 5, 6 mol/L), respectively. The higher the NaOH concentration was, the more obvious the characteristic peaks of LDH appeared

Table 2 The mineral components and chemical composition of boron mud and red mud

Boron mud	Mineral components	Muscovite	Forsterite	Huntite	Others			
	Content [wt %]	25	33	27	15			
	Chemical composition	MgO	Al_2O_3	Fe_2O_3	SiO_2	CaO	Na_2O	Loss
	Content [wt %]	37.6	2.22	7.59	18.1	3.48	0.909	28.5
Red mud	Mineral components	Muscovite	Quartz	Gibbsite	Calcite	Sodalite	Hematite	Goethite
	Content [wt %]	10	4	15	26	17	17	11
	Chemical composition	Al_2O_3	Fe_2O_3	SiO_2	TiO_2	CaO	Na_2O	Loss
	Content [wt %]	26.9	15.4	22.3	1.21	2.44	18.1	13.65

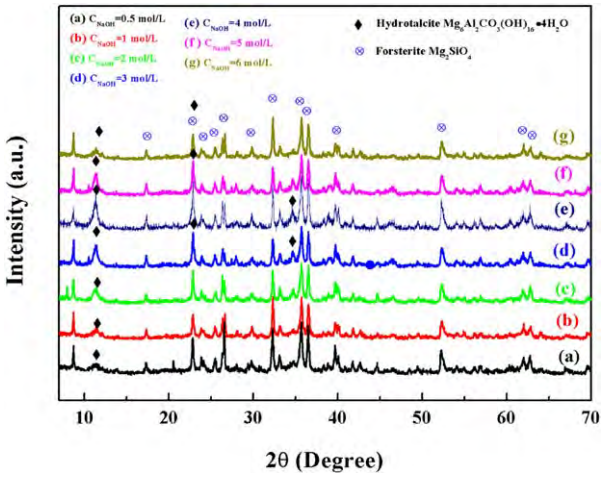

Fig. 2. XRD results of BR-LDH for different concentrations of NaOH. [Colour figure can be viewed at wileyonlinelibrary.com]

(when the NaOH concentration ranges from 0.5 to 4). However, the characteristic peaks of LDH became weaker as the pH increased from 4 to 6. Thus, a higher concentration of NaOH resulted in the unfavorable generation of LDH. According to these results, the prepared BR-LDH under this optimal conditions (the mass ratio = 4 : 1 and C_{NaOH} = 4 mol/L) were designated as OBR-LDH.

Characterisation of BR-LDH

SEM and energy-dispersive X-ray spectroscopy

Figure 3(a) and (b) depicted the boron mud and red mud micrographs, respectively. Figure 3(c)–(f) showed the SEM images of BR-LDH. The microstructures of BR-LDH were different for different mass ratios of boron mud to red mud at 2 mol/L NaOH. As shown in Fig. 3(d), the sheet structure of BR-LDH appeared. When the NaOH concentration increased from 2 (Fig. 3d) to 4 (Fig. 3e), the sheet structure became clearer. However, the sheet structure almost disappeared when the pH increased from 4 to 6. It was due to the fact that $Al(OH)_3$ could not precipitate with high NaOH concentration. The energy-dispersive X-ray spectroscopy (EDS) in Fig. 3(d) showed that the main elements were C

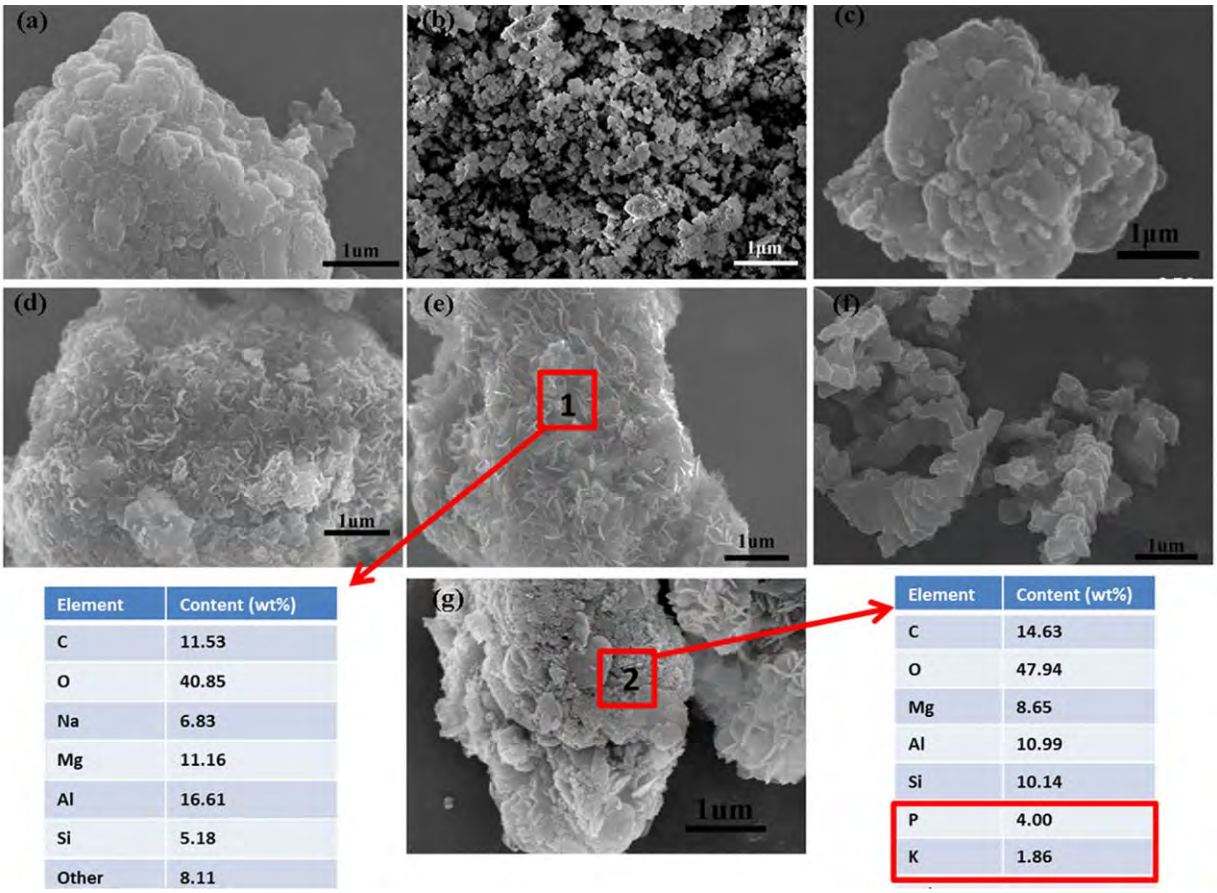

Element	Content (wt%)
C	11.53
O	40.85
Na	6.83
Mg	11.16
Al	16.61
Si	5.18
Other	8.11

Element	Content (wt%)
C	14.63
O	47.94
Mg	8.65
Al	10.99
Si	10.14
P	4.00
K	1.86

Fig. 3. SEM images of (a) boron mud, (b) red mud, (c) BR-LDH (dosage ratio = 1 : 1, C_{NaOH} = 2 mol/L), (d) BR-LDH (dosage ratio = 4 : 1, C_{NaOH} =2 mol/L), (e) BR-LDH (dosage ratio = 4 : 1, C_{NaOH} = 4 mol/L), (f) BR-LDH (dosage ratio = 4 : 1, C_{NaOH} = 6 mol/L), (g) BR-LDH after adsorption (dosage ratio = 4 : 1, C_{NaOH} = 4 mol/L). The selected area EDS of BR-LDH is shown in (f) and (g). [Colour figure can be viewed at wileyonlinelibrary.com]

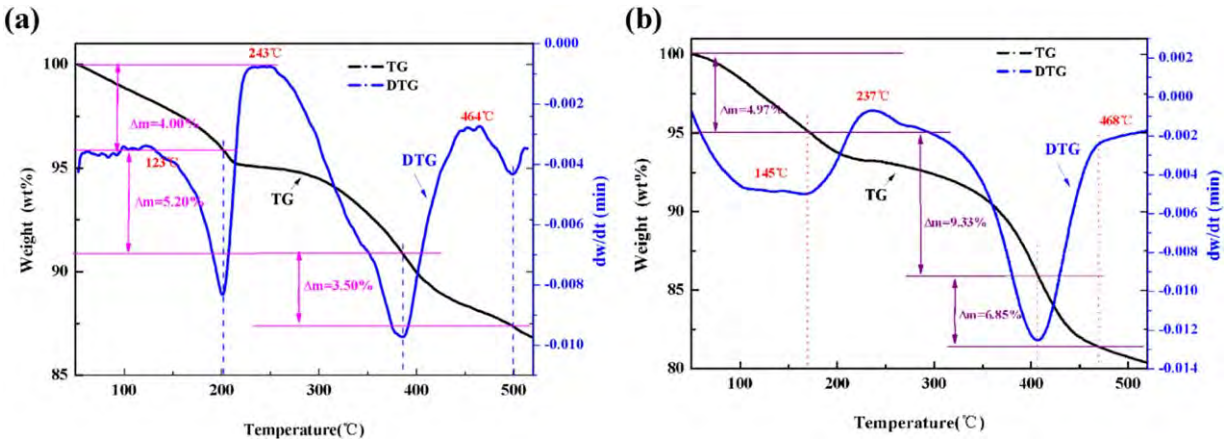

Fig. 4. TG-DTG of (a) BR-600 and (b) OBR-LDH. [Colour figure can be viewed at wileyonlinelibrary.com]

(11.53%), O (40.85%), Mg (11.16%) and Al (16.61%) on the surfaces of BR-LDH and these elements were also the main components of LDH. Thus, it indicated that LDH was successfully prepared using boron mud and red mud. Figure 3(g) showed the SEM of BR-LDH (mass ratio = 4 : 1, C_{NaOH} = 4 mol/L) after adsorption, indicating some pollutants attached on the surface of BR-LDH. The EDS analysis of BR-LDH after phosphate adsorption in Fig. 3(g)

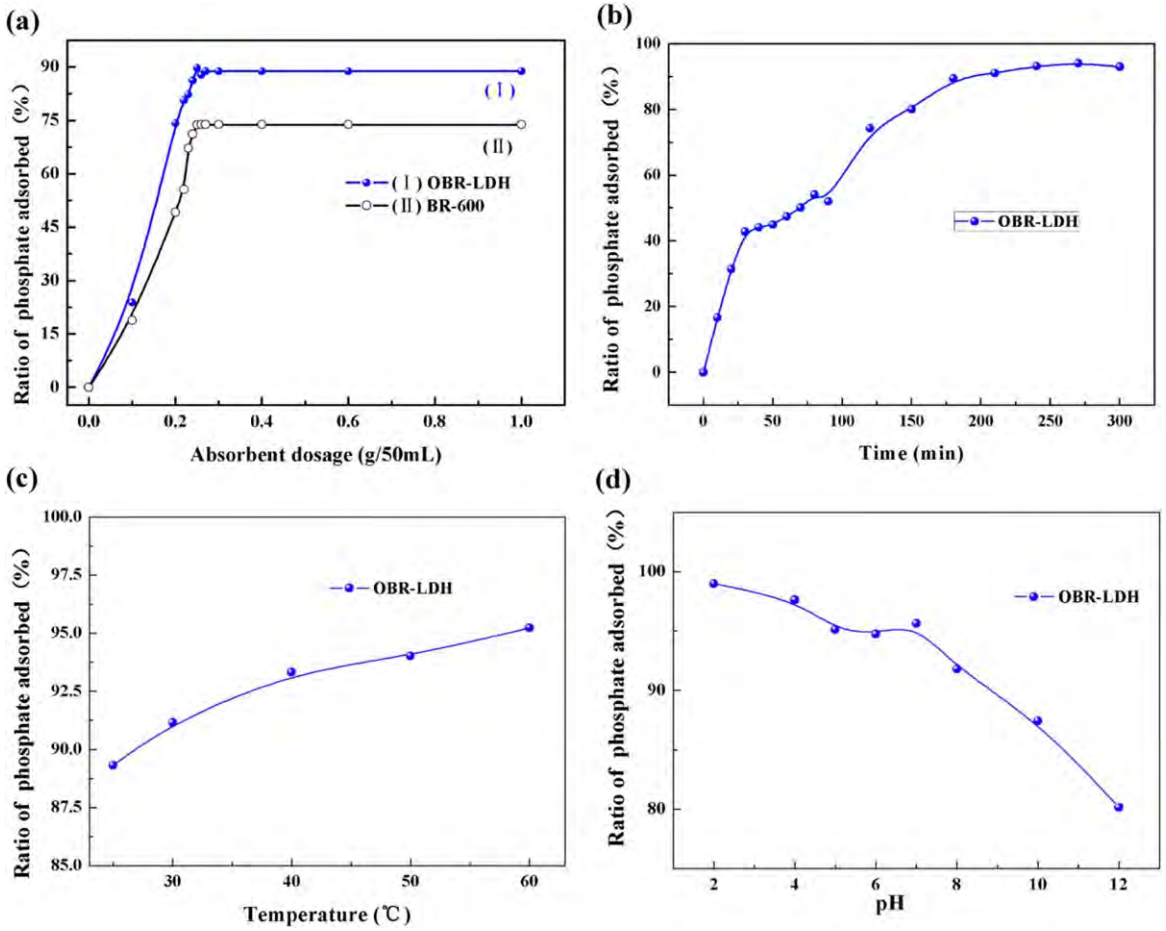

Fig. 5. Effects of phosphate adsorbed by OBR-LDH: (a) Different absorbent dosage, (b) different contact time, (c) different temperatures and (d) different pH. [Colour figure can be viewed at wileyonlinelibrary.com]

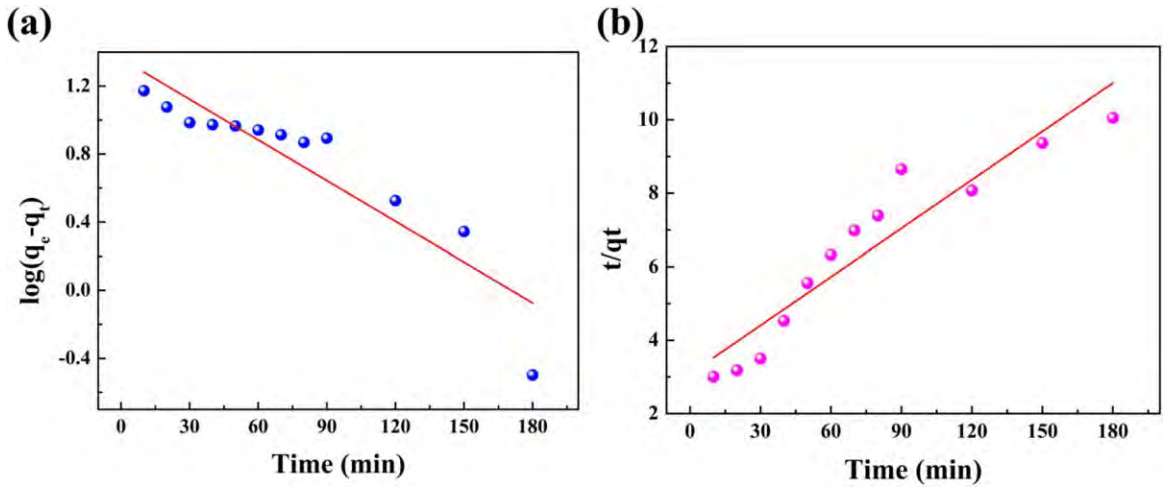

Fig. 6. (a) Pseudo-first-order and (b) Pseudo-second-order kinetics model plots for adsorption of phosphate on OBR-LDH. [Colour figure can be viewed at wileyonlinelibrary.com]

confirmed the presence of phosphorus and potassium and the adsorption of phosphate to BR-LDH.

Thermo-gravimetric-differential thermal analysis

Figure 4(a) showed the thermo-gravimetric-differential thermal analysis (TG-DTG) plots of BR-600. In the DTG pattern three mass loss steps were observed at 123, 243 and 464°C with mass losses of 4.00, 5.20 and 3.50%. The first stage was mainly attributed to the elimination of physically adsorbed water molecules. The second stage at 243°C and the third stage at 464°C were ascribed to the loss of adsorbed water and dehydration, respectively.

Figure 4(b) showed the TG-DTG plots of representative BR-LDH exhibiting three stages in the weight loss with increased temperature. Three mass loss steps were observed at 145, 237 and 468°C with mass losses of 4.97, 9.33 and 6.85%, respectively. The first stage at 145°C could be resolved into two overlapped processes and mainly ascribed to the elimination of physically adsorbed and interlayered water molecules. The second and third loss stemmed at 237 and 468°C from the loss of hydroxyl groups from the brucite-like layer along with interlayer carbonate ions with concomitant destruction of the layered structure (Reichle *et al*. 1986; Frost *et al*. 2007). The overall thermal behavior of BR-LDH was agreement with that reported for MgAl-LDH samples (Frost *et al*. 2006; Wang *et al*. 2013). The results of TG-DTG further illustrated that LDH had been successfully prepared by calcination of mixed boron mud and red mud under the basic medium.

Adsorption of phosphate by BR-LDH

The BR-LDH prepared under the optimal preparation conditions (mass ratio of boron mud to red mud = 4 : 1 and C_{NaOH} = 4 mol/L) was designated as OBR-LDH and adsorption experiments are performed.

Different adsorbent dosages were studied at 298 K for 3 h in water and phosphate solutions (100 mg/L). As shown in Fig. 5(a), the ratio of phosphate adsorbed by BR-600 (I) and OBR-LDH (II) reached equilibrium when the dosage is 0.25 g/50 mL. The ratios of phosphate adsorption reached 71.17 and 86.18%, respectively. It indicated that OBR-LDH possessed higher adsorption ability than BR-600 for phosphate and 0.25 g/50 mL was the experimentally determined optical absorbent dosage.

Figure 5(b) showed the effects of the contact time on adsorption of phosphate at the dosage of 0.25 g/50 mL. Phosphate adsorption was very fast at the beginning of the adsorption experiments. At 30 min, the adsorption process gradually slowed down. The adsorption processes reached equilibrium after 200 min. The maximum ratio of phosphate adsorption was 89.51%. The results were in agreement with previous studies indicating fast initial oxyanion adsorption by Mg/Al-LDH followed by a slower process until reaching equilibrium (Hu *et al*. 2014). Owing to the positive charges of the layer, OBR-LDH interacted strongly with anionic species in the medium and anion removal took place by two different mechanisms: (a) adsorption on the external surface and (b) anion exchange (Wei *et al*. 2011). The adsorption process was faster than anion exchange due to the strong interactions between negative ions and the positive external surface, while ion exchange was a diffusion process.

Table 3 Kinetic models parameters obtained in adsorption of phosphate on OBR-LDH

		pseudo first-order			pseudo second-order		
Adsorbent	$q_{e,exp}$	$q_{e,cal}$	k_f	R^2	$q_{e,cal}$	k_f	R^2
OBR-LDH	18.22	22.99	0.0184	0.82023	19.73	0.627	0.87972

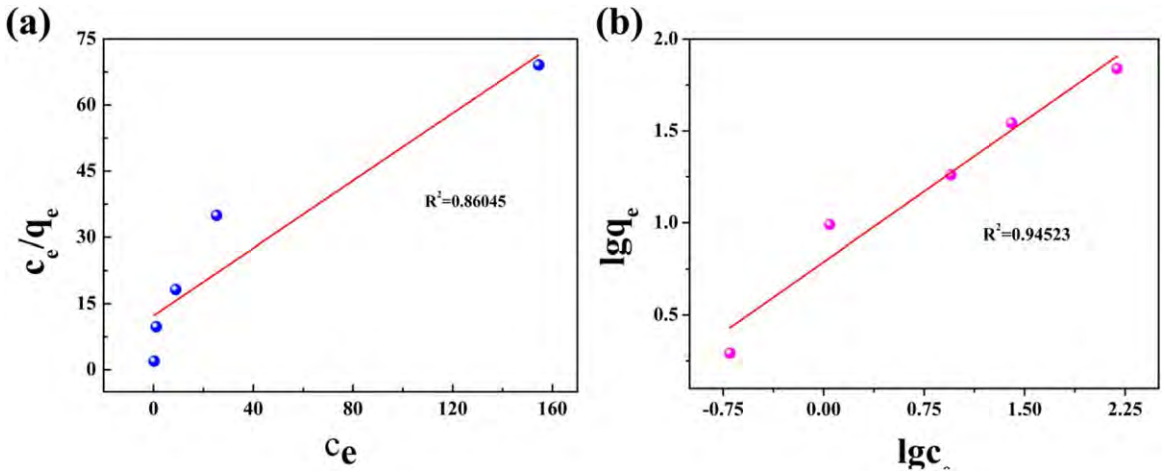

Fig. 7. (a) Langmuir and (b) Freundlich plots for adsorption of phosphate on OBR-LDH. [Colour figure can be viewed at wileyonlinelibrary.com]

Figure 5(c) showed that the ratio of phosphate adsorption increased with temperature in this range. It could be explained by that adsorption process was endothermic (Kannamba *et al*. 2010). The interaction between molecules in the layers of OBR-LDH became stronger as the temperature went up and the ratio of phosphate adsorption reached 95.4% at 60°C.

The pH of the aqueous solution was an important parameter to adsorption. Figure 5(d) showed the ratio of phosphate adsorbed on OBR-LDH at different pH. The ratio of phosphate adsorption on OBR-LDH was higher under acidic conditions than alkaline conditions. The ratio of phosphate adsorption decreased slowly when the pH rises from 1 to 7 due to the higher mobility of H^+ in the solution. OBR-LDH tended to adsorb phosphate on the surface at the moment. When the pH was higher than 7, a large amount of OH^- adsorbed on OBR-LDH, resulted in less phosphate adsorption. The ratio of phosphate adsorption was more than 93% at pH = 6–9, so the solution pH did not necessary to adjust in practical applications.

Adsorption kinetics

In order to study the adsorption kinetics of phosphate on OBR-LDH, the pseudo-first-order and pseudo-second-order kinetic models are tested. The linear form of the pseudo-first-order (3) and pseudo-second-order (4) equation are expressed as follows (Ho & Mckay 1999):

$$log\,(q_e - q_t) = log q_e - \frac{k_f}{2.303}t \tag{3}$$

$$\frac{t}{q_t} = \frac{1}{k_2 q_e^2} + \frac{1}{q_e}t \tag{4}$$

where k_f (L/min) is the rate constant of pseudo-first order adsorption. q_e (mg/g) and q_t (mg/g) are the amounts of phosphate adsorbed on the adsorbents at equilibrium and at time t (min), respectively. k_2 (g/(mg·min)) is the pseudo-second-order constant, and k_f and q_e for OBR-LDH can be determined from the plot of log (q_e – q_t) versus t in Fig. 6(a). The values of q_e and k_2 can be determined experimentally from the slope and intercept of the plot $\frac{t}{q_t}$ versus t in Fig. 6(b). The parameters and correlation coefficients were presented in Table 2. As shown in Fig. 6 and Table 3, the correlation coefficients R^2 of the pseudo-second-order expression was larger than that of the pseudo-first-order expression.

Table 4 Freundlich and Langmuir constants and correlation coefficients for adsorption of phosphate on OBR-LDH

	Langmuir			Freundlich		
Adsorbent	q_m	b	R^2	n	k_f	R^2
OBR-LDH	2.615	0.0312	0.860	1.270	3.244	0.945

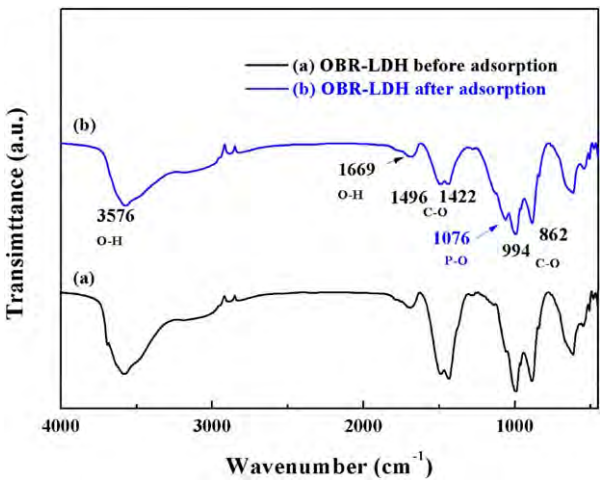

Fig. 8. FT-IR results: (a) OBR-LDH before adsorption and (b) OBR-LDH after adsorption. [Colour figure can be viewed at wileyonlinelibrary.com]

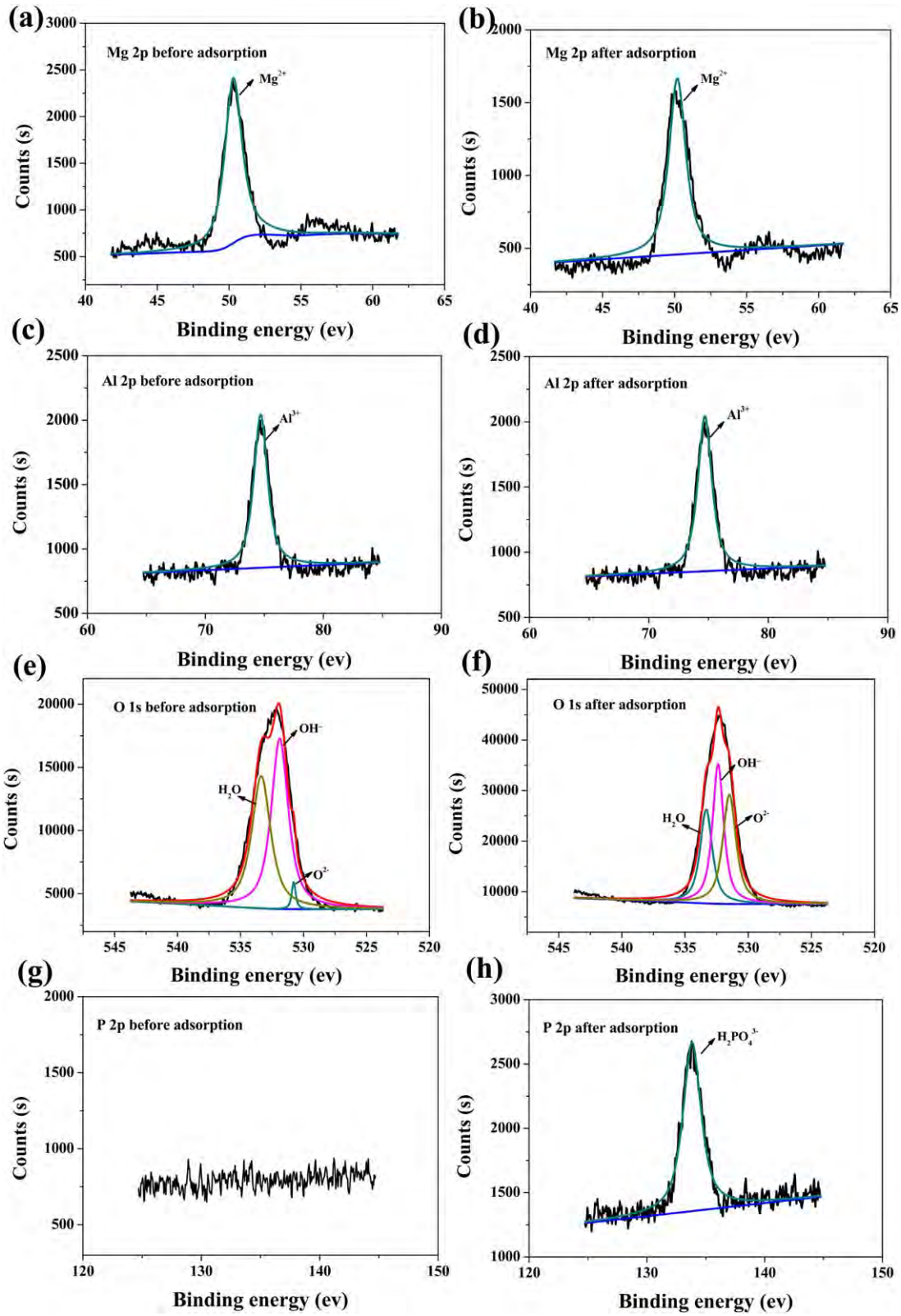

Fig. 9. XPS of OBR-LDH before and after adsorption. [Colour figure can be viewed at wileyonlinelibrary.com]

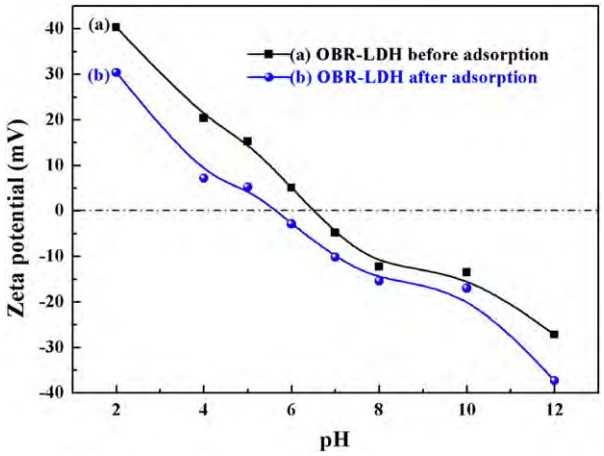

Fig. 10. Zeta potentials of (a) OBR-LDH before adsorption and (b) OBR-LDH after adsorption. [Colour figure can be viewed at wileyonlinelibrary.com]

The calculated adsorption capacity ($q_{e,cal}$) estimated by the pseudo-first-order model differed substantially to the experimental values, whereas the $q_{e,cal}$ values calculated from the pseudo-second-order kinetics model were very close to the experimental data. Moreover, the correlation coefficients R^2 for the pseudo-second-order model was much larger than that of the pseudo-first-order model (Mandal *et al*. 2014).

Adsorption isotherms

The equilibrium adsorption isotherm is fundamental to the behavior between the solution and adsorbent and important to the design of the adsorption system. The adsorption capacities at different aqueous equilibrium concentrations could be illustrated by the adsorption isotherms. Under the optimal preparation conditions, the adsorption isotherms of the two types of OBR-LDH for phosphate were studied at room temperature and the results were shown in Fig. 7. The adsorption equilibrium data of phosphate on OBR-LDH were processed according to the well-known two equilibrium models: Langmuir (6) and Freundlich (7) and the results were presented in Table 4.

$$\frac{c_e}{q_e} = \frac{1}{bq_m} + \frac{c_e}{q_m} \tag{6}$$

$$\log q_e = \log\ K_f + \frac{1}{n} \log c_e \tag{7}$$

where c_e (mg/L) are the equilibrium concentrations of phosphate adsorbed on the adsorbents. q_e (mg/g) and q_m (mg/g) are the adsorption capacity at equilibrium and at any time t (min), respectively. b (L/mg) is the Langmuir adsorption equilibrium constant related to the rate of adsorption. K_f ((mg/g)/(mg/L)$^{1/n}$) and n are the Freundlich constant and intensity factors, respectively (Xiang *et al*. 2010).

According to the values of R^2 in Table 3, the mathematical fit was better for the Freundlich isotherm than Langmuir isotherm. The calculated value of n (>1) in the Freundlich equation indicated a favorable adsorption process and adsorption was mainly multilayer adsorption.

Adsorption mechanism

In order to explain the interaction mechanisms between phosphate and OBR-LDH, FT-IR, XPS, Zeta potential determination and XRD were conducted on OBR-LDH before and after adsorption in Figs 8–10 and 11, respectively.

As shown in Fig. 8, the broad and intense adsorption bands at 3436 cm^{-1} (O–H stretching vibration) and 1631 cm^{-1} (O–H bending vibration) indicated the presence of interstitial water molecules. The peaks at 1496, 1422, 994 and 862 cm^{-1} were the characteristic absorption peaks of C–O, implying the presence of CO_3^{2-} species in the interlayer of OBR-LDH (Labajos *et al*. 1991). The peak at 1076 cm^{-1} was attributed to the bending vibration of adsorbed phosphate P–O (Liu *et al*. 2008). It indicated that $H_2PO_4^-$ had entered the interlayer of OBR-LDH.

To further explain the adsorption mechanism, the XPS of OBR-LDH before and after adsorption were conducted. As shown in Fig. 9, the Mg 2p and Al 2p were located at 50.34 and 74.40 eV in OBR-LDH before and after adsorption. It indicated that Mg(II) and Al(III) oxidation state were in the precipitates. The O 1s peak resulted in three peaks with the Gaussian shape, corresponding to O^{2-}, OH^- and H_2O, respectively. The peak of P 2p after adsorption appeared at 133.76 eV, illustrated that P in the form of $H_2PO_4^-$ was present in the OBR-LDH. It further indicated that $H_2PO_4^-$ had entered the interlayer of OBR-LDH (Wu *et al*. 2012).

The zeta potentials before and after adsorption were shown in Fig. 10. The isoelectric points (pH_{zpc}) of OBR-LDH

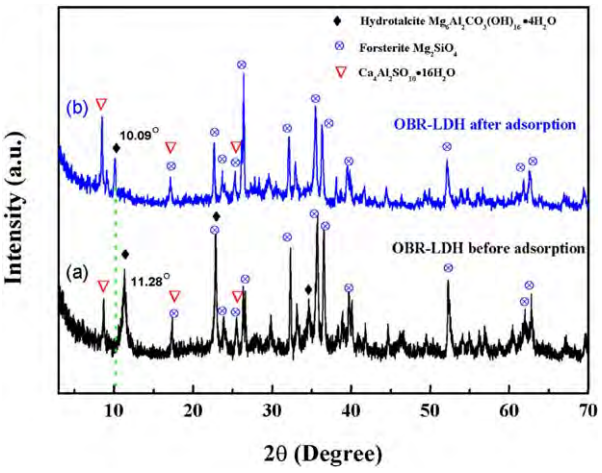

Fig. 11. XRD of (a) OBR-LDH before adsorption and (b) OBR-LDH after adsorption. [Colour figure can be viewed at wileyonlinelibrary.com]

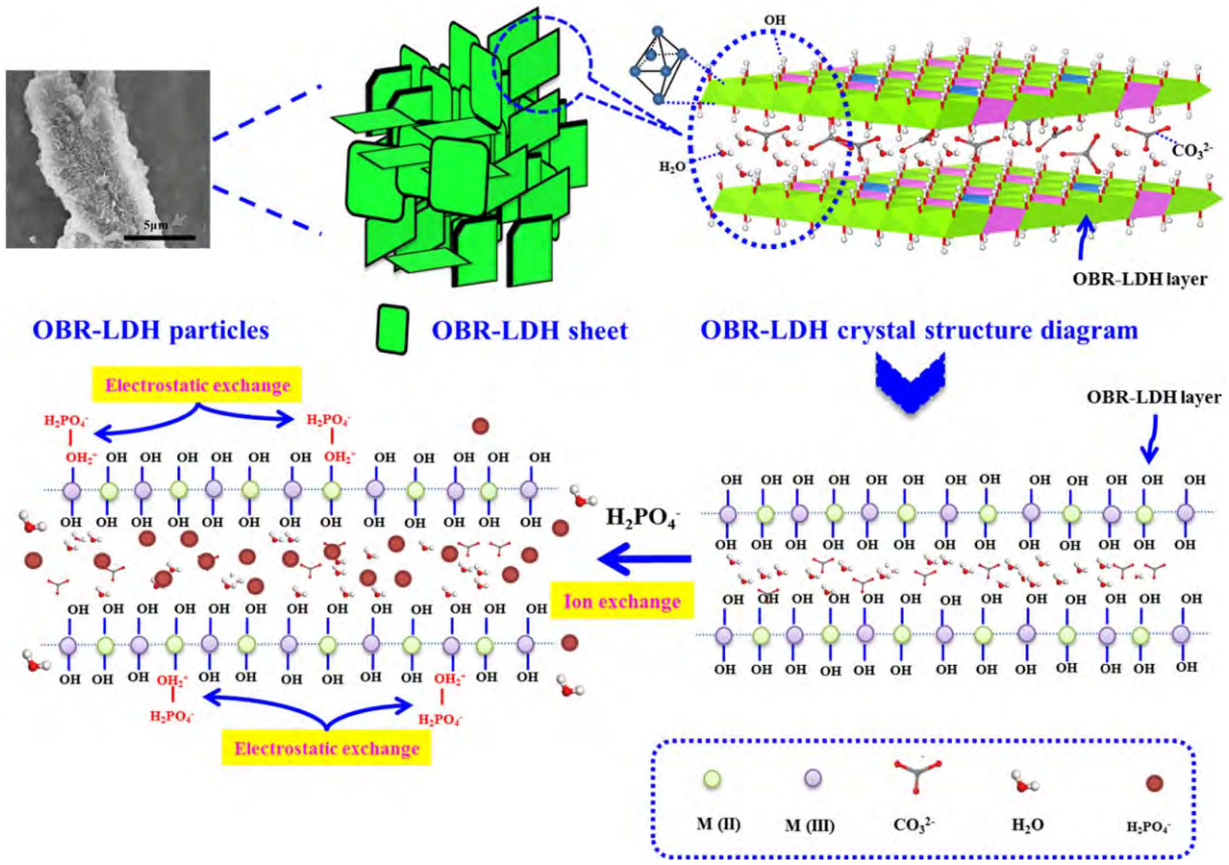

Fig. 12. Schematic diagram illustrating the possible adsorption mechanism on OBR-LDH. [Colour figure can be viewed at wileyonlinelibrary.com]

were determined by the pH when the zeta potential was zero to 6.84. After phosphate adsorption, the zeta potential of OBR-LDH decreased at different pH values and the pH_{zpc} shifted to 5.73. The solution pH was lower than pH_{zpc} of OBR-LDH (<6.84). The surface hydroxyl groups became protonated ($-OH_2^+$) and attracted negatively charged phosphate anions $H_2PO_4^-$. As the pH increased, the zeta potentials of OBR-LDH decreased. When the solution pH raised to 6.84, the surface of OBR-LDH was negatively charged. The electrostatic repulsion between the negatively charged surface sites and electronegative phosphate species resulted in less phosphate adsorption. This was in agreement with Fig. 5(d). Through the above analysis, the electrostatic attraction also played an important role in phosphorus adsorption (Yang *et al*. 2014).

The XRD patterns of OBR-LDH before and after adsorption were shown in Fig. 11. The peak of hydrotalcite shifted from 11.28° to 10.09°. It indicated that phosphate was adsorbed in the hydrotalcite layers and replaced interlayer ions, leading to larger layer space. However, in Figs (1 and 2) and 11, the peaks of Forsterite and $Ca_4Al_2SO_{10}{\cdot}16H_2O$ were almost no changes. Meanwhile, compared to BR-600 of 71.17%, the ratio of phosphate adsorbed of OBR-LDH increased to 86.18% in Fig. 5(a). It showed that better adsorption effect was because of the formation of hydrotalcite.

Phosphate species were adsorbed by electrostatic attraction, ligand exchange, and ion exchange (Chitrakar *et al*. 2006; Mcbride 1994). According to zeta potentials (Fig. 10), the negatively charged phosphate species ($H_2PO_4^-$) could be

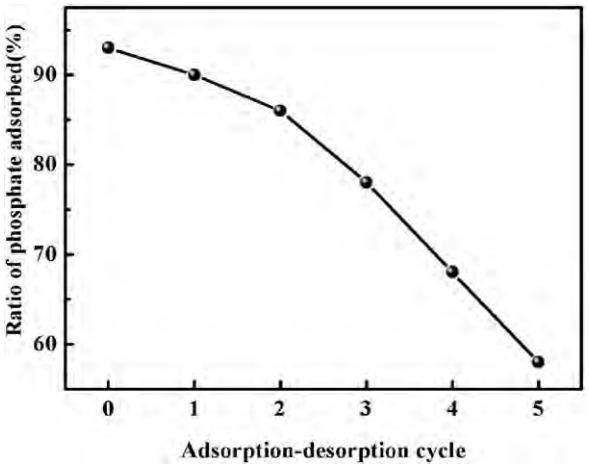

Fig. 13. The adsorption–desorption cycle of OBR-LDH.

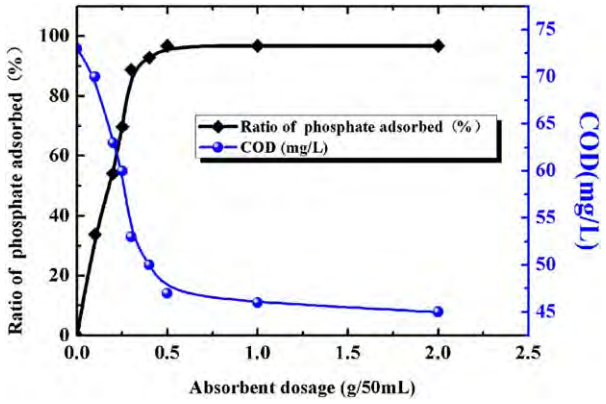

Fig. 14. The phosphate uptake and COD removal ratio of real wastewater by OBR-LDH. [Colour figure can be viewed at wileyonlinelibrary.com]

attracted electrostatically by the electropositive adsorbent surface since the solution pH was below the pH_{zpc} of OBR-LDH. The surface hydroxyl groups facilitated ligand exchange because $-OH_2^+$ could be more easily displaced from the metal binding sites than hydroxyl groups at a low pH (Xue *et al.* 2009). Ion exchange also occurred between the interlayer anions CO_3^{2-} and phosphate species. Thus, adsorption of phosphate species was postulated to proceed by three steps as illustrated in Fig. 12: (1) transfer of phosphate from the aqueous solution to sites on the OBR-LDH, (2) electrostatic attraction at the active sites and (3) ion exchange between the interlayer CO_3^{2-} and phosphate species.

Adsorption–desorption experiment

In order to determine the regenerability of OBR-LDH for its subsequent application as an adsorbent, the material was subjected to repeated adsorption–desorption cycles. In the present study, OBR-LDH saturated with phosphate were treated with 0.1 mol/L Na_2CO_3 solution. After that, the treated OBR-LDH as washed with doubly distilled water to remove any excessive CO_3^{2-} ions until the pH was in the range of 7.0–8.0. The regeneration efficiency was studied up to five adsorption–desorption cycles and the results are presented in Fig. 13. When the adsorption–desorption cycles were less than 2, the ratio of phosphate adsorbed of the regenerated OBR-LDH were still higher than 80% and had the good adsorption capacity. It indicated that the OBR-LDH could be recycled.

Phosphate removal from real effluent

In the actual process, the real wastewater usually contained inorganic, organics, heavy metals or microorganisms and their presence might have a great influence on final treatment effect. The real wastewater from Qinghe sewage treatment plant was used to study the phosphate removal by OBR-LDH and the results were showed in Fig. 14. When adsorbent dosage was 0.5 g/50 mL, the ratio of phosphate adsorbed (%) could reach 96.81%, and the concentration of soluble phosphate decreased from 3.6 to 0.11 mg/L. Meanwhile, the COD of the real wastewater also decreased from 73 to 47 mg/L. The results indicated the OBR-LDH could remove phosphate from the real wastewater and have potential application in the treatment of the real wastewater from sewage treatment plant.

Conclusion

OBR-LDH was successfully prepared when the mass ratio of boron mud to red mud and C_{NaOH} were 4 : 1 and 4 mol/L, respectively. The XRD and SEM showed that the prepared OBR-LDH had typical characteristics of LDH. The pseudo-second-order model accurately described the phosphate adsorption kinetics for the prepared OBR-LDH. The mathematical fit was better for the Freundlich isotherm than Langmuir isotherm and indicated adsorption was mainly multilayer adsorption. The FT-IR, XPS, Zeta potential determination and XRD indicated the electrostatic attraction, ion exchange and replacement of surface hydroxyl groups by phosphate were mainly responsible for phosphate adsorption by OBR-LDH. At the adsorbent dosage of 0.25 g/50 mL, contact time of 200 min, the temperature of 60°C, and pH of 6–9, the ratio of phosphate adsorbed could reach 93%. The adsorption–desorption experiment indicated the OBR-LDH can be recycled. The result of the actual experimental wastewater showed the ratio of phosphate adsorbed (%) could reach 96.81% at 0.5 g/50 mL of adsorbent dosage and the treatment effect was very obvious. In short, the OBR-LDH based on the boron mud and red mud was a good phosphate adsorbent and had high potential in reducing wastes, treating water and protecting the environment.

Acknowledgements

This work was supported by the National High Technology Research and Development Program of China [863 Program, 2012AA06A109]. City University of Hong Kong Strategic Research Grant (SRG) [No. 7004188], and City University of Hong Kong Applied Research Grant (ARG) [No. 9667085].

To submit a comment on this article please go to http://mc.manuscriptcentral.com/wej. For further information please see the Author Guidelines at wileyonlinelibrary.com

References

Atar, N., Olgun, A., Wang, S. and Liu, S. (2011) Adsorption of Anionic Dyes on Boron Industry Waste in Single and Binary

Solutions Using Batch and Fixed-Bed Systems. *J. Chem. Eng. Data*, **56**, 1596–1600.
Auerbach, S.M., Carrado, K.A. and Dutta, P.K. (2004) *Handbook of layered materials*. Marcel Dekker, New York.
Chitrakar, R., Tezuka, S., Sonoda, A., Sakane, K., Ooi, K. and Hirotsu, T. (2006) Phosphate Adsorption on Synthetic Goethite and Akaganeite. *J. Colloid Interface Sci.*, **298**, 602–608.
Das, J., Patra, B.S., Baliarsingh, N. and Parida, K.M. (2006) Adsorption of Phosphate by Layered Double Hydroxides in Aqueous Solutions. *Appl. Clay Sci.*, **32**, 252–260.
Delaney, P., Mcmanamon, C., Hanrahan, J.P., Copley, M.P., Holmes, J.D. and Morris, M.A. (2011) Development of Chemically Engineered Porous Metal Oxides for Phosphate Removal. *J. Hazard. Mater.*, **185**, 382–391.
Deng, L., Shi, Z., Li, B., Yang, L., Luo, L. and Yang, X. (2014) Adsorption of Cr(VI) and Phosphate on Mg–Al Hydrotalcite Supported Kaolin Clay Prepared by Ultrasound-Assisted Coprecipitation Method Using Batch and Fixed-Bed Systems. *Ind. Eng. Chem. Res.*, **53**, 7746–7757.
Drizo, A., Forget, C., Chapuis, R.P. and Comeau, Y. (2006) Phosphorus Removal by Electric Arc Furnace Steel Slag and Serpentinite. *Water Res.*, **40**, 1547–1554.
Frost, R.L., Musumeci, A.W., Kloprogge, J.T., Adebajo, M.O. and Martens, W.N. (2006) Raman Spectroscopy of Hydrotalcites with Phosphate in the Interlayer: Implications for the Removal of Phosphate from Water. *J. Raman Spectrosc.*, **37**, 733–741.
Frost, R.L., Musumeci, A.W., Adebajo, M.O. and Martens, W. (2007) Using Thermally Activated Hydrotalcite for the Uptake of Phosphate from Aqueous Media. *J. Therm. Anal. Calorim.*, **89**, 95–99.
Gök, A., Gök, M.K., Aşçı, Y.S. and Lalikoglu, M. (2014) Equilibrium, Kinetics and Thermodynamic Studies for Separation of Malic Acid on Layered Double Hydroxide (LDH). *Fluid Phase Equilib.*, **372 (372**), 15–20.
Guo, Y., Zhang, Y., Huang, H., Meng, K., Hu, K., Hu, P., Wang, X., Zhang, Z. and Meng, X. (2014) Novel Glass Ceramic Foams Materials Based on Red Mud. *Ceram. Int.*, **40**, 6677–6683.
Håkanson, L., Bryhn, A.C. and Hytteborn, J.K. (2007) On the Issue of Limiting Nutrient and Predictions of Cyanobacteria in Aquatic Systems. *Sci. Total Environ.*, **379**, 89–108.
Hesselmann, R.P.X., Rummell, R.V. and Resnlck, S.M. (2000) Anaerobic Metabolism of Bacteria Performing Enhanced Biological Phosphate Removal. *Water Res.*, **34**, 3487–3494.
Ho, Y.S. and Mckay, G. (1999) Pseudo-Second Order Model for Sorption Processes. *Process Biochem.*, **34**, 451–465.
Hu, P., Zhang, Y., Lv, F., Wang, X., Wei, F., Meng, X. and Jiang, S. (2014) Organic Pollution Removal from TNT Red Water Using Cu-Impregnated Activated Coke. *Water Air Soil Pollut.*, **225**, 1–10.
Huang, W., Wang, S., Zhu, Z., Li, L., Yao, X., Rudolph, V. and Haghseresht, F. (2008) Phosphate Removal from Wastewater Using Red Mud. *J. Hazard. Mater.*, **158**, 35–42.
Kannamba, B., Reddy, K.L. and Apparao, B.V. (2010) Removal of Cu(II) from Aqueous Solutions Using Chemically Modified Chitosan. *J. Hazard. Mater.*, **175**, 939–948.
Karageorgiou, K., Paschalis, M. and Anastassakis, G.N. (2007) Removal of Phosphate Species from Solution by Adsorption onto Calcite Used as Natural Adsorbent. *J. Hazard. Mater.*, **139**, 447–452.
Khitous, M., Salem, Z. and Halliche, D. (2015) Removal of Phosphate from Industrial Wastewater Using Uncalcined MgAl-NO Layered Double Hydroxide: Batch Study and Modeling. *Desalin. Water Treat.*, **57**, 1–12.
Labajos, F.M., Rives, V. and Ulibarri, M.A. (1991) Effect of Hydrothermal and Thermal Treatments on the Physicochemical Properties of Mg-Al Hydrotalcite-Like Materials. *J. Mater. Sci.*, **27**, 1546–1552.
Li, B., Zhang, Y., Zhou, X., Liu, Z., Liu, Q. and Li, X. (2016) Different Dye Removal Mechanisms Between Monodispersed and Uniform Hexagonal Thin Plate-Like MgAl–CO 3 2- -LDH and its Calcined Product in Efficient Removal of Congo Red from Water. *J. Alloys Compd.*, **673**, 265–271.
Liao, L., Ning, Z. and Xia, Z. (2012) Hydrothermal Synthesis of Mg–Al Layered Double Hydroxides (LDHs) from Natural Brucite and Al(OH) 3. *Mater. Res. Bull.*, **47**, 3897–3901.
Liu, H., Sun, X., Yin, C. and Hu, C. (2008) Removal of Phosphate by Mesoporous ZrO2. *J. Hazard. Mater.*, **151**, 616–622.
Liu, J., Duan, C., Zhou, J., Li, X., Qian, G. and Xu, Z.P. (2013) Adsorption of Bacteria onto Layered Double Hydroxide Particles to Form Biogranule-Like Aggregates. *Appl. Clay Sci.*, **75–76**, 39–45.
Mandal, S., Sahu, M.K., Giri, A.K. and Patel, R.K. (2014) Adsorption Studies of Chromium (VI) Removal from Water by Lanthanum Diethanolamine Hybrid Material. *Environ. Technol.*, **35**, 817–832.
Maurice, S.O., Dalibor, K., Mitsuhiro, K. and Hitoki, M. (2007) Adsorptive Removal of Phosphate Ions from Aqueous Solution Using Synthetic Zeolite. *Ind. Eng. Chem. Res.*, **46**, 894–900.
Mcbride, M.B. (1994) *Environmental Chemistry of Soils*. Oxford University Press, Oxford.
Morris, J.M., Jin, S. and Cui, K. (2008) Removal of Endocrine Active Compounds Using Layered Double Hydroxide Material. *Water Sci. Technol.*, **145** (58), 597−602.
Mustafa, S., Zaman, M.I. and Khan, S. (2006) pH Effect on Phosphate Sorption by Crystalline MnO 2. *J. Colloid Interface Sci.*, **301**, 370–375.
Nijboer, R.C. and Verdonschot, P.F.M. (2004) Variable Selection for Modelling Effects of Eutrophication on Stream and River Ecosystems. *Ecol. Modell.*, **177**, 17–39.
Noeline, B.F., Manohar, D.M. and Anirudhan, T.S. (2005) Kinetic and Equilibrium Modelling of lead(II) Sorption from Water and Wastewater by Polymerized Banana Stem in a Batch Reactor. *Sep. Purif. Technol.*, **45**, 131–140.
Onyango, M.S., Kuchar, D., Kubota, M. and Matsuda, H. (2009) Adsorptive Removal of Phosphate Ions from Aqueous Solution Using Synthetic Zeolite. *Ind. Eng. Chem. Res.*, **46**, 894–900.
Ozacar, M. (2003) Adsorption of Phosphate from Aqueous Solution onto Alunite. *Chemosphere*, **51**, 321–327.
Peleka, E.N. and Deliyanni, E.A. (2009) Adsorptive Removal of Phosphates from Aqueous Solutions. *Desalination*, **245**, 357–371.
Reichle, W.T., Kang, S.Y. and Everhardt, D.S. (1986) The Nature of the Thermal Decomposition of a Catalytically Active Anionic Clay Mineral. *J. Catal.*, **101**, 352–359.

Rojas, R. (2014) Copper, Lead and Cadmium Removal by Ca Al Layered Double Hydroxides. *Appl. Clay Sci.*, **87**, 254–259.

Roques, H., Nugroho-Jeudy, L. and Lebugle, A. (1991) Phosphorus Removal from Wastewater by Half-Burned Dolomite. *Water Res.*, **25**, 959–965.

Seida, Y. and Nakano, Y. (2002) Removal of Phosphate by Layered Double Hydroxides Containing Iron. *Water Res.*, **36**, 1306–1312.

Tillotson, S. (2006) Phosphate Removal: An Alternative to Chemical Dosing. *Filtr. Sep.*, **43**, 10–12.

Wang, S., Li, Z. and Chao, L. (2015) Polyethyleneimine as a Novel Desorbent for Anionic Organic Dyes on Layered Double Hydroxide Surface. *J. Colloid Interface Sci.*, **458**, 315–322.

Wang, X., Bai, Z., Zhao, D., Chai, Y., Guo, M. and Zhang, J. (2013) New Synthetic Route to Mg-Al-CO_3 Layered Double Hydroxide Using Magnesite. *Mater. Res. Bull.*, **48**, 1228–1232.

Wang, X., Zhang, Y., Lu, R., Zhou, F., An, Q., Meng, Z., Fei, B. and Lv, F. (2014a) Novel Multiple Coagulant from Bayer Red Mud for Oily Sewage Treatment. *Desalin. Water Treat.*, **54**, 1–9.

Wang, X., Zhang, Y., Lv, F., An, Q., Lu, R., Hu, P. and Jiang, S. (2014b) Removal of Alkali in the Red Mud by SO2 and Simulated Flue Gas Under Mild Conditions. *Environ. Prog. Sustain. Energy.*, **34**, 81–87.

Wei, F., Zhang, Y., Lv, F., Chu, P.K. and Ye, Z. (2011) Extraction of Organic Materials from Red Water by Metal-Impregnated Lignite Activated Carbon. *J. Hazard. Mater.*, **197**, 352–360.

Wu, Y., Ying, Y., Ji, Z.Z., Liu, J., Ying, C., Zhi, P.X. and Qian, G. (2012) Effective Removal of Pyrophosphate by Ca-Fe-LDH and its Mechanism. *Chem. Eng. J.*, **179**, 72–79.

Xiang, C., Huang, X., Wang, X. and Sun, D. (2010) Influence of Calcination on the Adsorptive Removal of Phosphate by Zn-Al Layered Double Hydroxides from Excess Sludge Liquor. *J. Hazard. Mater.*, **177**, 516–523.

Xue, Y., Hou, H. and Zhu, S. (2009) Characteristics and Mechanisms of Phosphate Adsorption onto Basic Oxygen Furnace Slag. *J. Hazard. Mater.*, **162**, 973–980.

Yan, L.G., Xu, Y.Y., Yu, H.Q., Xin, X.D., Qin, W. and Du, B. (2010) Adsorption of Phosphate from Aqueous Solution by Hydroxy-Aluminum, Hydroxy-Iron and Hydroxy-Iron–Aluminum Pillared Bentonites. *J. Hazard. Mater.*, **179**, 244–250.

Yang, K., Yan, L.G., Yang, Y.M., Yu, S.J., Shan, R.R., Yu, H.Q., Zhu, B.C. and Du, B. (2014) Adsorptive Removal of Phosphate by Mg–Al and Zn–Al Layered Double Hydroxides: Kinetics, Isotherms and Mechanisms. *Sep. Purif. Technol.*, **124 (124**), 36–42.

Yin, Y., Zhang, Y., Zhen, Z., Chu, P.K., Lv, F. and Ji, J. (2013) Thermal Degradation and Flame Retarding Characteristics of Polypropylene Composites Incorporated with Boron Mud. *Compos. Sci. Technol.*, **85**, 131–135.

Zeng, L., Li, X. and Liu, J. (2004) Adsorptive Removal of Phosphate from Aqueous Solutions Using Iron Oxide Tailings. *Water. Res.*, **38**, 1318–1326.

Zhang, L., Xiong, Z., Li, L., Burt, R. and Zhao, X.S. (2016) Uptake and Degradation of Orange II by Zinc Aluminum Layered Double Oxides. *J. Colloid Interface Sci.*, **469**, 224–230.

Zhao, D., Sheng, G., Hu, J., Chen, C. and Wang, X. (2011) Adsorption of Pb(II) on Mg_2Al Layered Double Hydroxide. *Chem. Eng. J.*, 171, 167–174.

Zhao, Y., Li, N. and Xia, S. (2016) Polyamide Nanofiltration Membranes Modified with Zn–Al Layered Double Hydroxides for Natural Organic Matter Removal. *Compos. Sci. Technol.*, **132**, 84–92.